IEEE Access
Multidisciplinary ⋮ Rapid Review ⋮ Open Access Journal

Received July 15, 2020, accepted July 20, 2020, date of publication August 17, 2020, date of current version September 18, 2020.

Digital Object Identifier 10.1109/ACCESS.2020.3016981

A Highly-Efficient Fuzzy-Based Controller With High Reduction Inputs and Membership Functions for a Grid-Connected Photovoltaic System

LOTFI FARAH[1], AMIR HUSSAIN[2], (Senior Member, IEEE), ABDELFATEH KERROUCHE[2], (Member, IEEE), COSIMO IERACITANO[3], JAMIL AHMAD[4], (Senior Member, IEEE), AND MUFTI MAHMUD[5], (Senior Member, IEEE)

[1]Genie Électromécanique Laboratory, Electromécanique Department, Badji Mokhtar University, Annaba 23000, Algeria
[2]School of Computing, Edinburgh Napier University, Edinburgh EH10 5DT, U.K.
[3]DICEAM, Mediterranea University of Reggio Calabria, 89124 Reggio Calabria, Italy
[4]Institute of Information Technology, Kohat University of Science and Technology (KUST), Kohat 26000, Pakistan
[5]Department of Computing and Technology, Nottingham Trent University, Nottingham NG11 8NS, U.K.

Corresponding author: Lotfi Farah (lotfi.farah@univ-annaba.dz)

The work of Amir Hussain was supported by the UK Engineering and Physical Sciences Research Council (EPSRC) under Grant EP/M026981/1, Grant EP/T021063/1, and Grant EP/T024917/1.

ABSTRACT Most conventional Fuzzy Logic Controller (*FLC*) rules are based on the knowledge and experience of expert operators: given a specific input, *FLCs* produce the same output. However, *FLCs* do not perform very well when dealing with complex problems that comprise several input variables. Hence, an optimization tool is highly desirable to reduce the number of inputs and consequently maximize the controller performance, leading to easier maintenance and implementation. This article, presents an enhanced fuzzy logic controller applied to a photovoltaic system. Specifically, both inputs and membership functions are reduced, resulting in a Highly Reduced Fuzzy Logic Controller (*HRFLC*), to model a 100kW grid-connected Photovoltaic Panel (*PV*) as part of a Maximum Power Point Tracking (*MPPT*) scheme. A *DC* to *DC* boost converter is included to transfer the total energy to the grid over a three-level Voltage Source Converter (*VSC*), which is controlled by varying its duty cycle. *FLC* generates control parameters to simulate different weather conditions. In this study, only one input representing the current variation ($\triangle I$) of the *FLC* is used to provide an effective and accurate solution. This reduction in simulation inputs results in a novel *HRFLC* which simplifies the solar electric system design with output Membership Functions (*MFs*). Both are achieved by grouping two rules instead of using an existing state-of-the-art method with twenty-five *MFs*. To the best of our knowledge, this is the first *FLC* able to provide such rules compression. Finally, a comparison with different techniques such as Perturb and Observe (*P&O*) shows that *HRFLC* can improve the dynamic and the steady state performance of the *PV* system. Notably, experimental results report a steady state error of 0.119%, a transient time of 0.28s and an *MPPT* tracking accuracy of 0.009s.

INDEX TERMS Boost converter, current variation, grid connection, high reduced fuzzy based *MPPT* controller (*HRFLC*), photovoltaic panel, three level *VSC*.

NOMENCLATURE

VARIABLES

$\triangle$E(t)	Error Variation
$\triangle$I	Current Variation
$\triangle$P	Power Variation
$\triangle$V	Voltage Variation
C	Capacitor Value
D	Duty Cycle
dP_{PV}/dI_{PV}	Power derivation by current
$E(t)$	Error
G	Irradiation
I_{in}	Input Current
I_{out}	Output Current
I_{Ph}	Photo Current
I_{PV}	Light Generated Current
L	Induction Value

The associate editor coordinating the review of this manuscript and approving it for publication was Salvatore Favuzza.

Le	VSC Level
N	IGBTs Number
R_o	Output Resistance
R_{eq}	Equivalent Resistance
R_{in}	Input Resistance
T	Temperature
V_o	DC/DC Output Voltage
V_{ab}	Output Line to Line Voltage of the VSC
$V_{carrier}$	Carrier Voltage
V_{in}	DC/DC Input Voltage
V_{PV}	Module Output Voltage
X_i	Input Fuzzy Data
Y_{COG}	Output Fuzzy Controller Value

ACRONYMS

ADC	Analogic to Digital Converter
AI	Artificial Intelligence
ANFIS	Adaptive Neuro Fuzzy Inference System
ANN	Artificial Neural Network
COG	Center Of Gravity
$DC-DC$	Direct Current to Direct Current
FIS	Fuzzy Inference System
FLC	Fuzzy Logic Controller
HC	Hill Climbing
Hi	High
HRFLC	Highly Reduced Fuzzy Logic Controller
IE	Initial Error
InCon	Incremental Conductance
Lo	Low
MF	Membership Function
Y_i	Membership Function Value
MPP	Maximum Power Point
MPPT	Maximum Power Point Tracking
NPC	Neutral Point Clamped
P&O	Perturb & Observe
P_{MPP}	Power value at the Maximum Power Point
P_{PV}	Panel Power
PB	Positive Big
PID	Proportional, Integral and Derivation
PS	Positive Small
PV	PhotoVoltaic
PVG	Photo Voltaic Generator
PWM	Power Wave Modulation
S&H	Sample and Hold
SSE	Steady State Error
ST	Steady Time
TOANC	Third Order Adaptative Neuro Fuzzy Controller
TrC	Triangular Carrier
TT	Tracking Time
VSC	Voltage Source Converter

CONSTANT

A	PV cell ideal factor
f	Frequency
I_{CSr}	Short Circuit Current
I_{mp}	Optimal Current
I_o	Saturation Current
k	Boltzmann Constant
N_P	Parallel connected cells Number in a PV Module
N_s	Series connected cells Number in a PV module
P_m	Maximal Module Power
q	The electron charge
R_s	Serial Resistance in PV Cell
R_{sh}	Parallel Resistance in PV Cell
V	Voltage Value
V_{dc}	Input VSC Voltage
V_{mp}	Optimal Voltage Module
V_{oc}	PV Module Open Circuit Voltage
V_{ref}	Reference Voltage

I. INTRODUCTION

In the last few years, there is a great deal of interest worldwide in searching new energy sources able to replace the dwindling fossil fuels. In this context, solar energy turned out to be the most attractive alternative due to its advantages of being cleaner, renewable and inexhaustible [1], [2]. The main function of Photovoltaic (*PV*) is to transform the solar irradiance into electric power. However, the generated power from *PV* depends not only on irradiance but also on other factors such as temperature and spectral properties of sunlight [3]–[5]. These conditions need to be controlled in order to allow a *PV* panel to operate at the Maximum Power Point (*MPP*). It is well known from *MPP* theory that the power delivered to the load is maximum only when the internal impedance is equal to the load impedance. For this reason, a *DC-DC* converter is used. In the literature, many techniques have achieved this adaptation between the *PV* panel and the load impedance at different atmospheric conditions such as the well-known Perturb and Observe (*P&O*) [3]–[6], including the Incremental Conductance technique *(InCon)*. *P&O* is cost effective and relatively easy to implement for controlling directions. However, this technique shows trade-offs between tracking speed and steady state accuracy to control atmospheric perturbations [3]–[7]. To overcome this problem, several solutions have been proposed [8]–[10]. In particular, it is worth mentioning that the perturbation step increases when the working point is far from the *MPP*, since the steps are proportional to the ratio dP_{PV}/dV_{PV} (and vice-versa) [8]–[11].

In the recent years, with the emergence and development of Artificial Intelligence (*AI*) [12], many applications such as, text mining to biology, financial forecasting, rehabilitation systems, trust management and medical diagnosis [13]–[15], [15], [17]–[21] have been efficiently improved. Furthermore, *AI* also provided effective and robust solutions to the field of electro-control systems by developing *PID*, fuzzy logic [11], [22]–[34], [36]–[38] and Artificial Neural Networks (*ANNs*) [39]–[41] based-control approaches. A comprehensive fuzzy system has been used by [11] to intelligently and adaptively tune the *PID* gain. Adaptive neuro-fuzzy controller system has been proposed for controlling *MPPT* with constant temperature and varying irradiance [22]–[25]. Recently, fuzzy logic is used in several applications due to its simplicity and its interpretability. Note that the main advantage of such technique is the addition or withdrawal of membership functions (*MFs*) without rehabilitation or re-learning. Fuzzy logic allows to model natural language rules and also complex dynamic systems. For this reason, fuzzy-based *MPPT* algorithms have gained a great deal of attention [11], [22]–[31]. Notably, high tracking performance have been obtained by using fuzzy-based *MPPT* [11], [22]–[31]. Hitherto, most of the works used two inputs and one output with five *MFs* to generate twenty-five rules [22]–[32]. Others used one output and two inputs of seven *MFs*, resulting in forty-nine rules [22]. In [23], two inputs were used with three *MFs*, yielding nine rules. Vicente Salas et al. [42] employed the variation of current as the unique input in *MPPT* controller. Specifically, the authors used one input with two *MFs*, one output with two *MFs* and only two rules. To the best of our knowledge, this was the first approach able to provide a significant reduction in number of inputs and *MFs*. It is to be noted, as reported in the literature, that different inputs can be selected. In particular, some used the temperature and irradiance variation [23], whereas others used error variation and momentum [24]–[28]. In [32], the proposed fuzzy controller employed different input variables, such as: (1) slope of solar power vs. solar voltage and slope changes; (2) slope and power variation ($\triangle P$); (3) $\triangle P$ and voltage variation ($\triangle V$); (4) $\triangle P$ and current variation ($\triangle I$); (5) sum of conductance and conductance increment; (6) sum of conductance arctangent angles and increment conductance arctangent. In [41] the inputs were dP_{PV}/dI_{PV} and the error *E(t)* (defined as P_{MPP} - P_{PV}); or, *E(t)* and error variation ($\triangle E(t)$). However, for computational reasons, the best inputs turn out to be the $\triangle P_{PV}$ and $\triangle V_{PV}$ (or $\triangle I_{PV}$), power variation and voltage (or current) variation, respectively [22]–[33], [39]–[41]. Hence, as reported in the aforementioned works, all controllers based on *MPPT* used at least two inputs. In contrast, this article propose a highly-efficiency fuzzy-based *MPPT* controller with high reduction inputs and *MFs* for a grid-connected photovoltaic system. Notably, only two *MFs* were used. Furthermore, $\Delta I_{PV} = (I_{PV}(k) - I_{PV}(k-1))$ is selected as unique input. Consequently, the calculation time, the number of variables and the circuitry (Analog to Digital Converter (*ADC*), Sample and Hold (*S&H*), filter, etc..) are significantly reduced. Moreover, the proposed fuzzy-based controller approach is able to decrease the tracking time and concurrently increase the tracking accuracy as compared with other state-of-the-art controllers.

The rest of the paper is organized as follows: in Section II mathematical details of a *PV* panel are introduced; in Section III the design of the *DC-DC* converter is presented; Section IV and V describe the fuzzy based *MPPT* controller and the Pulse Width Modulation (*PWM*) used for the three level voltage source converter, respectively. In Section VI the model and simulation of the *PV* system with *HRFLC* based *MPPT* controller is presented. In Section VII the experimental results are discussed and in Section VIII conclusions are addressed.

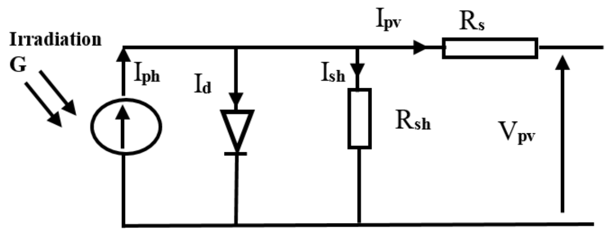

FIGURE 1. Circuit model of a photovoltaic cell [35].

II. MATHEMATICAL MODELING FOR A PHOTOVOLTAIC PANEL

A solar cell is composed of two types of semiconductors, called *p*-type and *n*-type. Photovoltaic transformation occurs when solar cell is exposed to sunlight, by converting the electromagnetic solar irradiance to electricity. Incident irradiance produces proportional electron-hole pairs if their energy is greater than the energy of the semiconductor's band-gap. Fig. 1 shows the circuit model of a standard photovoltaic model. The photocurrent I_{Ph} is the current source of the *PV* cell, generated when irradiation G occurs [42], [48]. Intrinsic shunt and series *PV* cell resistances are R_{sh} and R_s, respectively. It is to be noted that R_{sh} assumes typically high values and vice-versa, R_s low values. *PV* cells associated to larger units result in *PV* modules; these, interconnected together in parallel-series configurations, lead to the production of *PV* arrays. Equation (1) shows the current output when the mathematical model of the *PV* panel is simulated [43].

$$I_{PV} = N_P I_{Ph} - N_P * I_0[exp(\frac{q*(V_{PV}+I_{PV}R_s)}{(N_s AkT)}) - 1]. \quad (1)$$

In this work, the SunPower SPR-305-WHT *PV* panel is used with the following characteristics: Maximal Module Power (P_m) of 305W, optimal voltage (V_{mp}) of 54.7V, optimal current (I_{mp}) of 5.58A, saturation current (I_o) of $1.1753e^{-08}$A, photo-current (I_{Ph}) of 5.9602A, short circuit current (I_{CSr}) of 5.96A, open circuit voltage (V_{oc}) of 64.2V, serial resistance (R_s) of 0.037998Ω, parallel resistance (R_{sh}) of 993.51Ω and number of cells equal to 96. As regards the *PV* array, its characteristics are: serial modules number of 5 and parallel modules number of 66. Hence, the *PV* has a power of about 100kW, obtained as follows 66 × 5 × 305W = 100650W = 100.65kW. Irradiance of 1kW/m^2 and cell temperature of 25°C are the electrical specifications under test conditions. I-V and P-V curves of the array are depicted in Fig. 2. Here, the *PV* panel is directly connected to a *DC-DC* converter. This converter is an impedance adapter and allows to transfer the power captured from the *PV* panel to the grid toward a three-level voltage source converter.

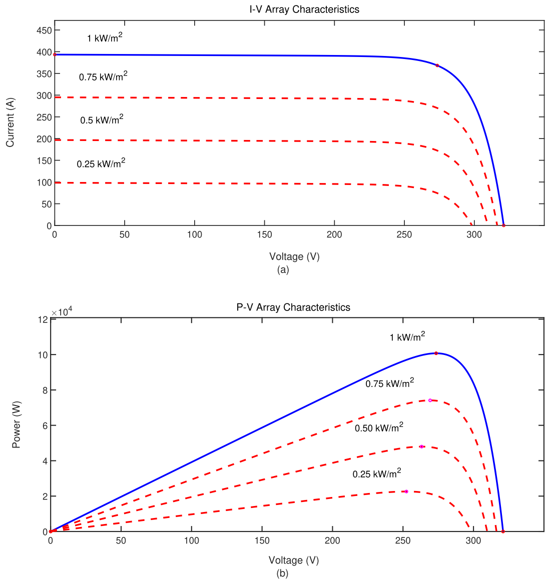

FIGURE 2. Array characteristics curves I-V (a) and P-V (b).

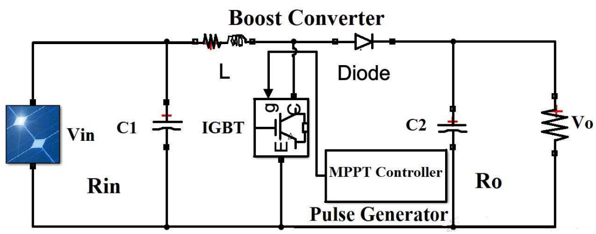

FIGURE 3. The DC-DC boost converter.

III. DESIGN THE DC-DC CONVERTER

A simple *DC-DC boost* converter transfers the power consumption from the *PV* Generator (*PVG*) to the load, when the adaptation condition (between *PVG* and load) occurs. The adaptation is characterized by an adequate duty cycle signal ($0 < D < 1$). Note that the *PWM* signal controls the valve gate, *IGBT*, in the boost converter. The wiring Simulink diagram of the *DC-DC* boost is shown in Fig. 3.

The relationship between inputs and outputs variables of the boost converter is represented by the following equations [44]:

$$V_o = V_{in}/(1 - D). \tag{2}$$

$$I_{out} = (1 - D)I_{in}. \tag{3}$$

whereas, Equation (4) shows the equivalent resistance (R_{eq}) of the *DC-DC* boost converter:

$$R_{eq} = R_{in}(1 - D)^2. \tag{4}$$

The maximum power is transferred to the load when R_{eq} is equal to the output resistance (R_o) of the *PV* system [45], [46]. Hence, according to the maximum power transfer theorem the duty cycle can be obtained as follows:

$$R_{in} = V_{in}/I_{in} = R_o(1 - D)^2 \Longrightarrow D = 1 - \sqrt{\frac{R_{in}}{R_o}}. \tag{5}$$

Inductor (L) and capacitor (C) functions of the *DC-DC* boost converter are instead defined as:

$$L = \frac{(V_o - V_{in})V_{in}}{f(\triangle I)V_o}. \tag{6}$$

$$C = \frac{(V_o - V_{in})I_{out}}{f(\triangle V)V_o}. \tag{7}$$

where D is the duty cycle; f is the frequency (5 kHz in this study); V_{in} and V_o are the inputs and outputs voltages, respectively; $\triangle I$ and $\triangle V$ are the current and voltage ripple. Here, $L = 5e^{-3}$H and $C = 12000e^{-06}$F. Fig. 4 depicts the I-V curve of the panel studied with different working zone. In particular, A-B area denotes the buck working zone, B-C the boost working zone and finally A-C the buck-boost working zone [47]. In this work, the boost converter's working zone (B-C) is the most important and, $\triangle I$ is the variable of greatest interest. Note that in Fig. 4, B is the *MPP* point and C is the open circuit point. At the B point $R_o = R_{in}$. Furthermore, in this area, $R_o \gg R_{in}$ with $R_{in} = R_o(1 - D)^2$. In order to have a stable voltage at the grid, the *VSC* voltage must be stable and constant. In this study, the voltage supplied to the *VSC* is kept constant ($V = 500$V) as shown in Fig. 10.

IV. FUZZY BASED MPPT CONTROLLER

A. FUZZY INFERENCE SYSTEM

A standard Fuzzy Inference System (*FIS*) consists of three modules, as shown in Fig. 6. In the first stage, called *fuzzification*, input variables are expressed in linguistic variables by assigning a *MF*. Secondly, *IF-THEN* rules are applied. Finally, in the *defuzzification* step, linguistic variables are transformed into specific output values and parameters are adjusted based on the input-output data relation [22]–[33].

B. FUZZY LOGIC CONTROLLER

A Fuzzy Logic Controller (*FLC*) is based on a *FIS* [32]. In fuzzification, the selected linguistic variables are the Positive Small (*PS*) and the Positive Big (*PB*). These linguistic values attribute a fuzzy score to the input. In this article, both input and output *MFs* are triangular for its simplicity and ease of implementation (Fig. 5). It is to be noted that a high number of *MFs* lead to an increase of rules and consequently, the control program is difficult to implement.

In this work, two rules are necessary to efficiently develop the control and provide accurate results. Moreover, only one input is used for the *FLC*, that is the current variation $\triangle I_{PV}$, defined as follows:

$$\triangle I_{PV}(n) = I_{PV}(n) - I_{PV}(n-1). \tag{8}$$

Table 1 reports the rules used in this article. As can be seen only two *MFs* are involved. In contrast, in [22]–[32] higher number of rules are employed (i.e., from 9 to 49). Note that the rules define the relationship between $\triangle I$ and D, represented by the IF-THEN instructions. For example, if the

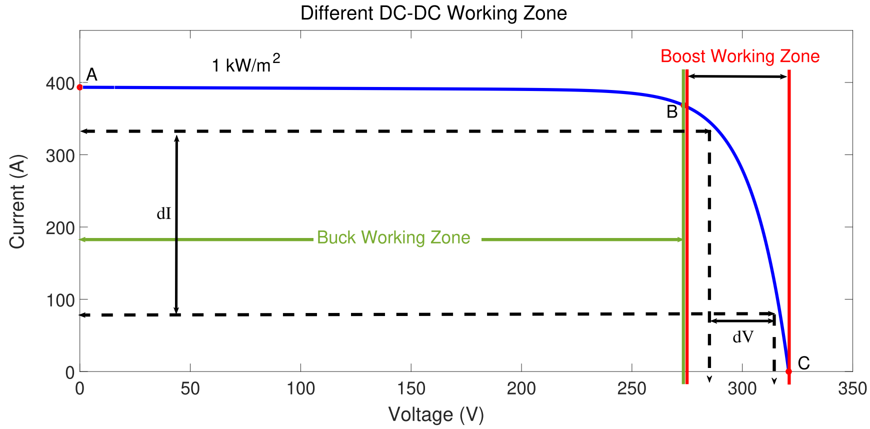

FIGURE 4. I-V curve of the working zone of the buck-boost converter.

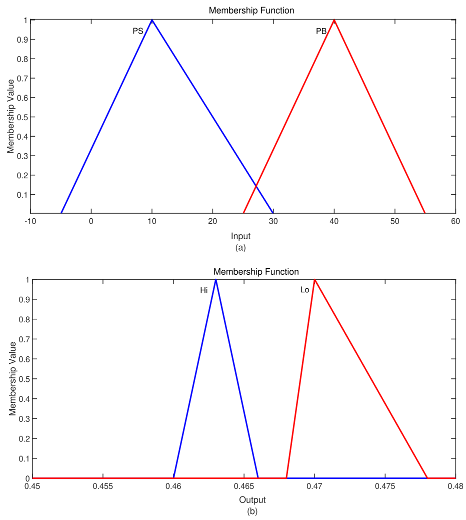

FIGURE 5. Input (a) and output (b) Fuzzy Membership Functions (MFs).

TABLE 1. Fuzzy rules.

$\triangle I_{PV}$	D
PS	Hi
PB	Lo

change in current is *PS* then *D* will be high.

$$Y_{COG} = \frac{\sum_{i=1}^{n} Y_i(X_i)X_i}{\sum_{i=1}^{n} Y_i(X_i)}. \tag{9}$$

where *COG* stands for Centre Of Gravity. The final level of *FLC* is the defuzzification able to produce a signal that controls the *MPP*. The *PV* panel current and the *PV* current variation $\triangle I$ are illustrated in Fig. 7. As can be seen, $\triangle I$ is always positive in all irradiance variations.

V. THREE LEVEL PWM VOLTAGE SOURCE CONVERTER

In the literature, several multilevel inverter topologies have been introduced, such as the diode clamped multilevel inverter, the flying capacitor multilevel inverters, and the cascaded H-bridge multilevel inverter. The most used is the well-known Neutral Point Clamped (*NPC*) [49], [50]. In this article, a three-level Voltage Source Converter (*VSC*) is employed, since it is suitable for higher voltage inverters and provides the following advantages than a common two-level inverters: i) low output current ripples; ii) reduced harmonic power as a result of a smaller output voltage that leads to cleaner AC output waveform; iii) the IGBTs are subjected to the half of the bus voltage; iv) the *NPC* inverter is characterized by a low common-mode and line-to-line voltage step. However, the three-level *VSC* provides a double effective switching frequency, an augmented number of IGBTs and a complex control strategy while increasing in level. This means that the cost and magnitude of its components is higher than the well-known two-level inverters, due to the reduced output voltage steps. In order to achieve such voltages, *N* IGBTs are added in each level:

$$N = 2(Le - 1). \tag{10}$$

where *Le* the desired level. In this study $Le = 3$, so, four IGBTs are needed for one leg, as shown in Fig. 8. In this topology, half of the voltage ($V_{dc}/2$) is applied to the IGBT achieved by the two equal capacitors in series. Furthermore, two clamp diodes in each leg are responsible for driving the half voltage to each specific IGBT [49]. For each of the three phases, produced in each leg (Fig. 8), the output voltage switches between $-\frac{V_{dc}}{2}$ and $\frac{V_{dc}}{2}$.

These voltages are obtained by turning on at the same time: 1) A1 and A2; 2) A2 and A3; 3) A3 and A4 as reported in Table 2, where A1, A2, A3 and A4 are the IGBTs in each leg. Such switching control options generate $\frac{V_{dc}}{2}$, zero and $-\frac{V_{dc}}{2}$. After filtering, a sine waveform is obtained at the AC output. The connection to the 0 Volt (neutral point) is assured by the clamp diodes D3 and D4. It can be seen from Table 2 that A2 and A3 conduct more than A1 and A4 causing a conduction loss on A2 and A3 and a switching loss on A1

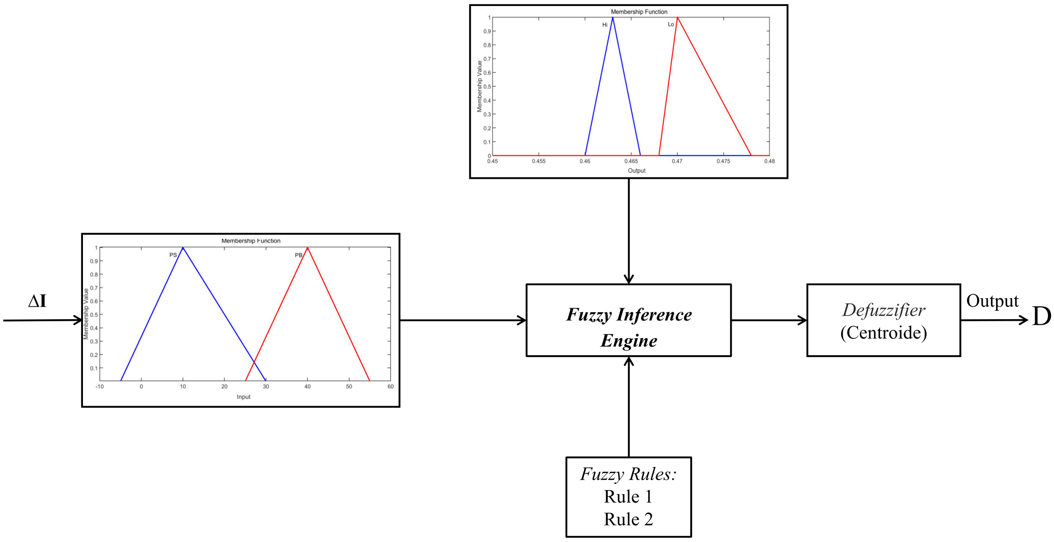

FIGURE 6. Proposed *HRFLC* based *MPPT* controller diagram.

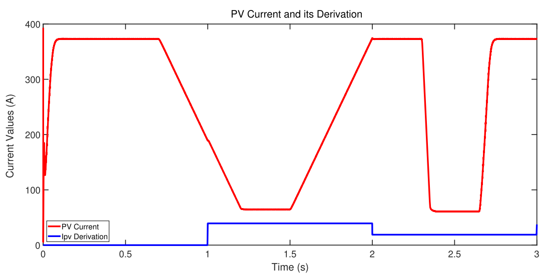

FIGURE 7. PV panel current and its derivation.

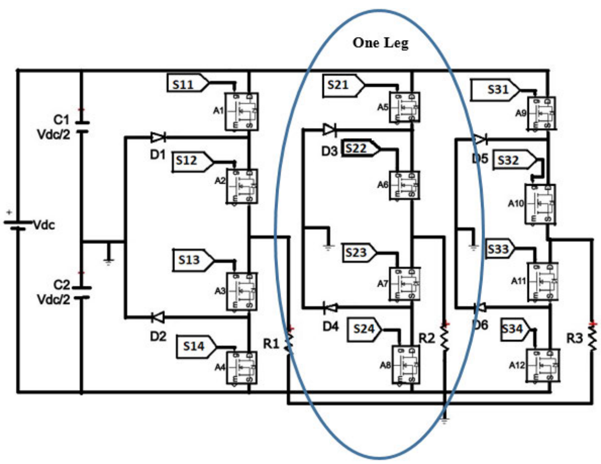

FIGURE 8. Three phase voltage source converter.

and A4 [50]. The capacitors C1 and C2 are coupled in series to generate the neutral point (0 Volt). Setting an equal voltage in the capacitors and establishing a neutral tension in the mid-point is important for the proper operation of *NPC*. Any unbalance voltage in the capacitors will affect directly the AC output. In this work, the sine triangular *PWM* waveform method is used [50], [51]. Specifically, in order to create the sine-carrier *PWM*, a comparison of the three references control signals, the pure sine waveform with 120°, and the two triangular carrier waves *TrC1* and *TrC2* is performed. Fig. 9 shows the comparison of one reference with the two triangular carriers. Specifically, the comparison of the sine waveform with *TrC1* and *TrC2* produces the on/off switch of A1 and A2, respectively. The switching on and off of A3 and A4 are the inverse of A1 and A2, respectively.

TABLE 2. IGBTs switching options.

IGBT				V_{out}
A1	A2	A3	A4	
1	1	0	0	$V_{dc}/2$
0	1	1	0	0
0	0	1	1	$-V_{dc}/2$

The corresponding control signals for the IGBTs can be expressed as follows:

$$V = \begin{cases} 1 & \text{if} \quad V_{carrier} > V_{ref} \\ 0 & \text{if} \quad V_{carrier} < V_{ref} \end{cases} \tag{11}$$

A zoom of the line-to-line voltage (V_{ab}), obtained at the *VSC*, is illustrated in Fig. 10. Here, the total harmonic distortion calculated for V_{ab} is 0.39%.

VI. MODELING AND SIMULATION OF PV SYSTEM WITH HRFLC BASED MPPT CONTROLLER

The simulation model of the incremental conductance technique was performed by using constant temperature and by varying irradiance. Fig. 11 depicts irradiance and temperature selected as input to the *PV* panel. Fig. 12 represents the proposed *HRFLC* of a *PV* panel connected to the grid. In particular, Fig. 12 (a) depicts the synoptic scheme of the panel connected to the grid toward the *VSC* with the High

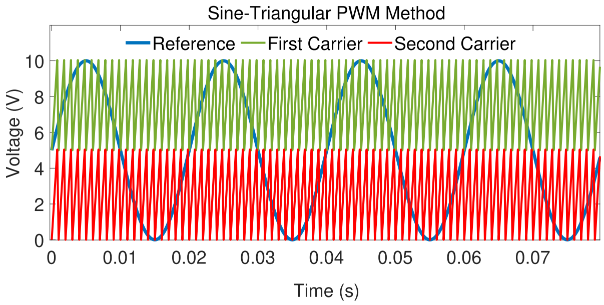

FIGURE 9. Comparison of the reference to two triangular carriers.

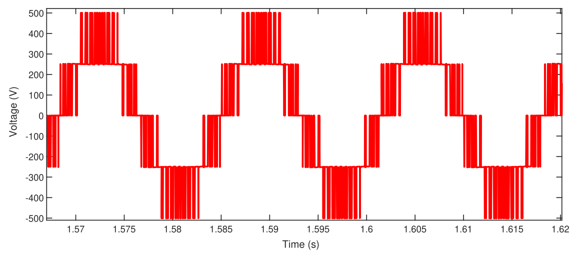

FIGURE 10. A zoom in VSC voltage V_{ab}.

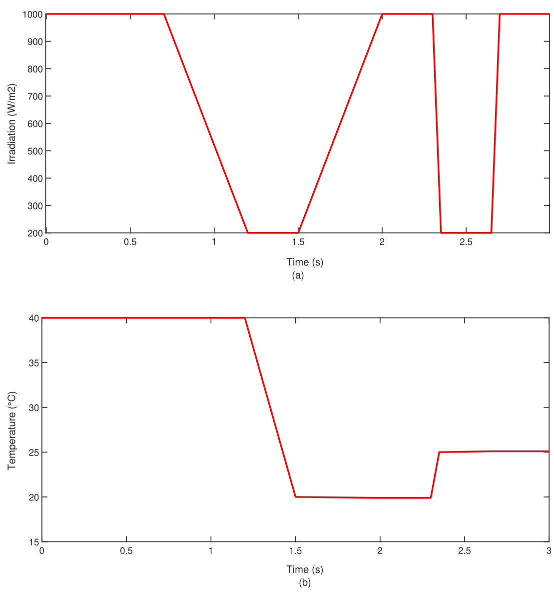

FIGURE 11. Irradiation (a) and temperature (b) as a function of time.

Reduced Fuzzy based *MPPT* controller; whereas, Fig. 12 (b) illustrates the global scheme of the *PV* panel connected to the grid toward the boost *DC-DC* converter and the *VSC*.

The power transfer between the *PV* panel and the boost *DC-DC* converter at 25°C is shown in Fig. 13 (a); while, comparison results with 40°C, 20°*C* are reported in Fig. 13 (b). The steady state error (*SSE*) and tracking time (*TT*) are shown in Fig. 14 and 15, respectively. Fig. 16 (a) depicts the Steady Time (*ST*), *SSE* and *TT* at 40°; whereas, Fig. 16 (b) highlights *ST*, *SSE* and *TT* at 20°C.

However, it is to be noted that a significant improvement was observed when the proposed *HRFLC* is employed. In particular, as regards the simulation carried out at 25°C, *TT*, *ST* and *SSE* were of 0.008s, 0.08s, 0.12 kW, respectively. This resulted in an error percentage of 0.12kW/100.65kW = 0.119%. In relation to the simulation at 20°C, instead, *TT*, *ST* and *SSE* were of 0.01s, 0.04s, 0.005kW, respectively. In this case the error percentage was of 0.005kW/100.65kW = 0.0049%. Finally, as regards the experiment at 40°C, *TT*, *ST* and *SSE* were of 0.01s, 0.22s, 0.01kW, respectively, achieving an error of 0.01kW/100.65kW = 0.0099% and an initial loss of about 9.5kW. The relationship between the boost power and grid power is depicted in Fig. 17. Specifically, Fig. 17(a) reports the simulation results at 25°C. In this scenario, *TT* is less than 0.004s (Fig. 19), *ST* is about 0.3s and *SSE* is of 100.54kW-98.83kW = 1.71kW (Fig. 18), providing an error percentage of 1.71kW/ 100.65kW = 1.69%. Results show high tracking efficiency and a good performance due to the use of the three level converter. Note that this performance can be improved when using five level converter or more. As regards simulation performed at 20°C as shown in Fig. 20(b), the *ST* is 0.02s, *TT* is 0.005s, *SSE* is 2kW, resulting in an error of 2kW/100.65kW = 1.98%. As regards the 40°C simulation (see Fig. 20(a)), the following errors 0.03s *TT*, 0.17s *ST* and 1.4kW *SSE* were achieved, resulting an error percentage of 1.4kW/100.65kW = 1.39%. It is to be noted that in 20°C simulation there is a gain in power due to the materials characteristics of the *PV*. In this work, a stable voltage (i.e., 500V) was used to supply the *VSC*. By this assumption, the power variation depends on the current. Hence, the power estimated at the grid is 98.83kW and the power of the boost is 100.54kW, as shown in Fig. 18. The global power transfer between the *PV* panel and the grid at 25°C is shown in Fig. 21. In this case, *TT* (Fig. 23), *ST* and *SSE* (Fig. 22) were of 0.005s, 0.09s and 1.82kW, respectively. For 20°C simulation, as shown in Fig. 24 (b) the *ST* was 0.02s, *TT* 0.02s, *SSE* 1.8kW, leading to an error percentage of 1.8kW/100.65kW = 1.78%. Finally, as regards the 40°C simulation (Fig. 24 (a)) reports 0.04s of *TT*, 0.17s *ST* and 1.4kW of *SSE*, resulting in an error of 1.4kW/100.65kW = 1.39%.

VII. EXPERIMENTAL RESULTS

In this article, a *HRFLC*-based *MPPT* controller connected to grid with only one input is developed. More specifically, here, the variation of irradiance and temperature in time has been taken into account. Note that three temperatures has been studied 40°C, 25°C, and 20°C. An excellent tracking between the power grid and the *PV* panel power was achieved as reported in Fig. 21, 22, 23 for the 25°C; in Fig. 24 (a) and Fig. 24 (b) for 40°C and 20°C, respectively. In addition, a complete adaptation was observed in the results related to the *PV* panel power and the boost power as illustrated in Figs 13, 14 and 15 for the 25°C; Fig. 16 (a) and 16 (b) for 40°C and 20°C, respectively. It is worth mentioning that a fast reaction and adaptation to different working conditions was observed. In Fig. 24 (a), with the proposed *HRFLC*,

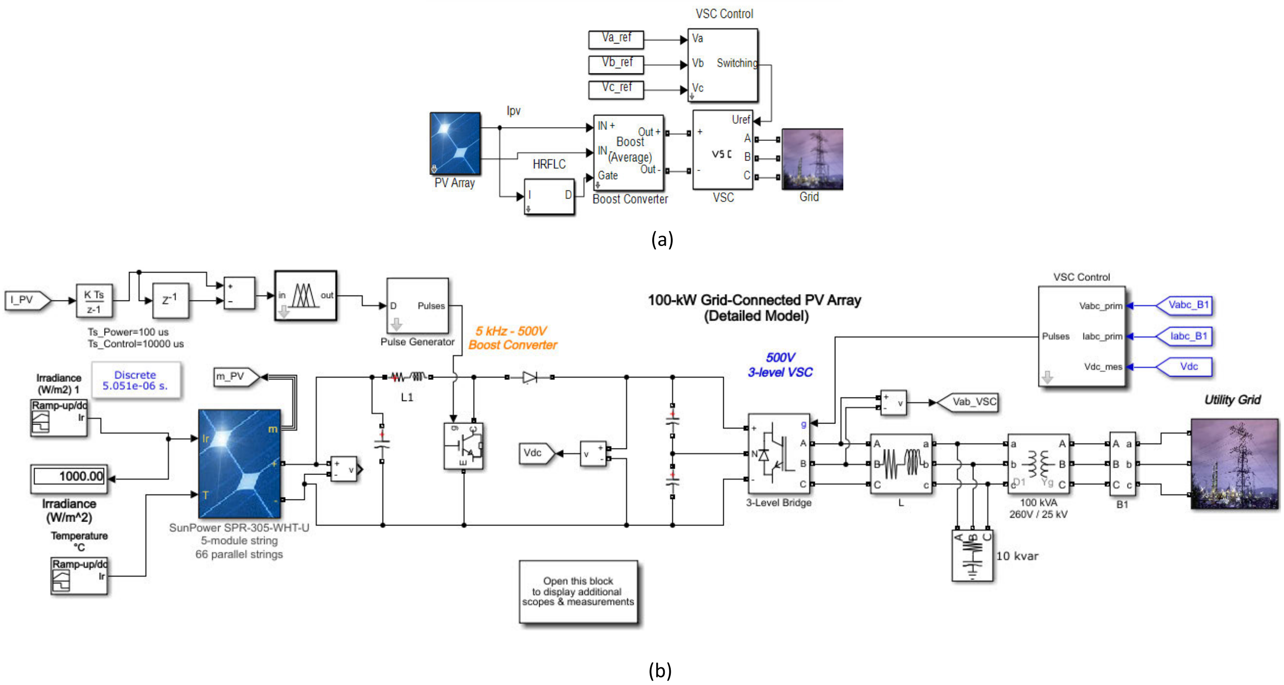

FIGURE 12. **(a) Synoptic scheme of the PV panel connected to grid. (b) PV panel connected to grid with the HRFLC.**

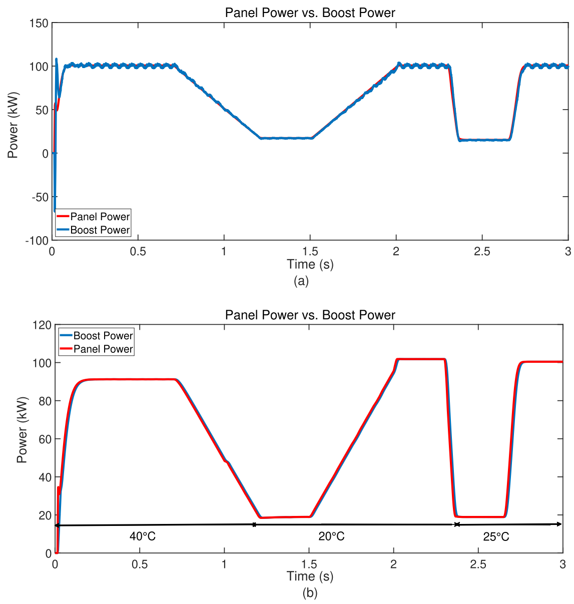

FIGURE 13. **Simulation results of panel power and boost power at 25°*C* (a) and 40°*C*, 20°*C*, 25°*C* (b).**

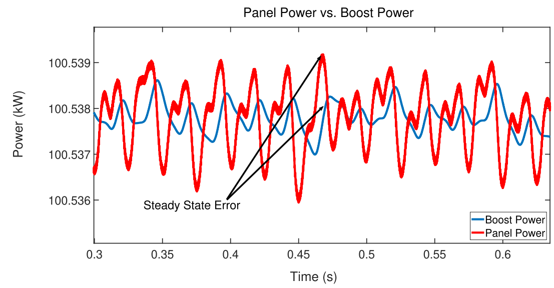

FIGURE 14. **Simulation results of the steady state error between the panel power and boost power at 25°*C*.**

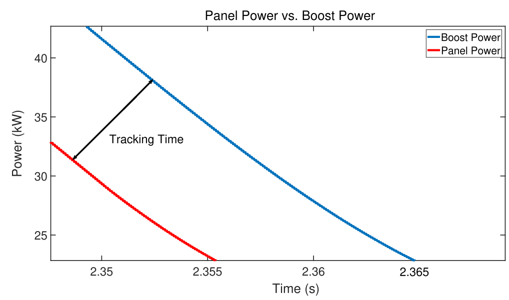

FIGURE 15. **Simulation results of the tracking time between panel power and boost power at 25°*C*.**

the efficiency was 98.83kW power transmission from the *PV* panel to grid out of 100.65 kW, meaning 98.19% of transmitted power for 25°C, 89.8kW for 40°C and 100.2kW for 20°C as illustrated in Fig. 24 (b). The variation of the duty cycle was between only two values: 0.463 and 0.478 to get the highest and lowest irradiance, respectively.

For the power transferred from the panel to the grid in the case of 25°C the tracking time error was about 0.005s as shown in Fig. 23. Fig. 22 depicts a steady state error of 1.82 kW and a steady time of about 0.09s. Since the panel power was 100.65kW, the steady state error was 1.8% (or 98.19% tracking efficiency). Hence, for 20°C and 40°C the tracking times were 0.02s and 0.04s respectively; whereas, the steady state error were 1.8kW and 1.4kW, respectively.

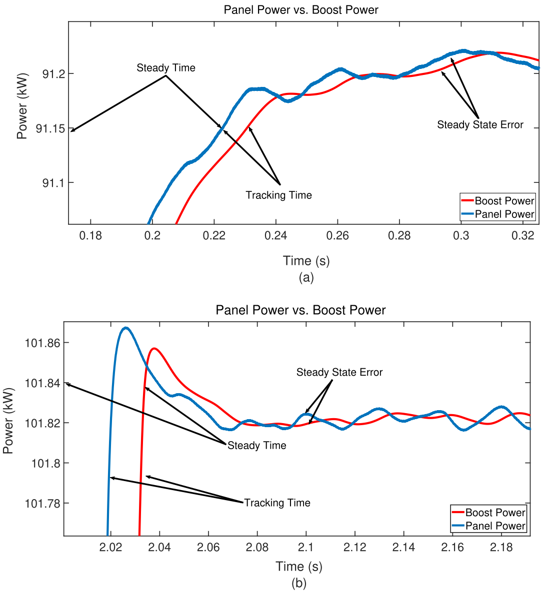

FIGURE 16. Errors between panel power and boost power at 40°C (a) and 20°C (b).

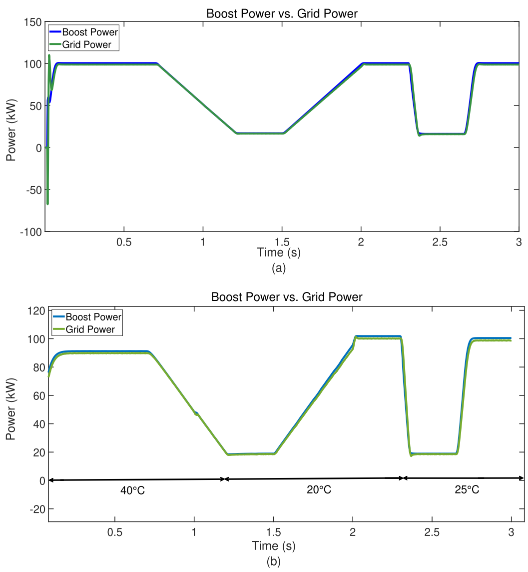

FIGURE 17. Simulation results of boost power and grid power at 25°*C* (a) and 40°*C*, 20°*C*, 25°*C* (b).

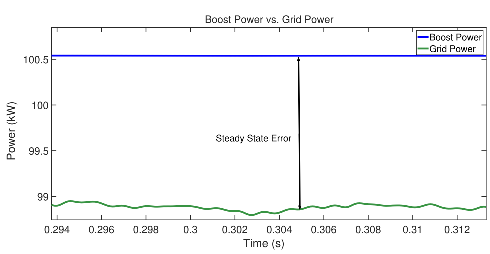

FIGURE 18. Simulation results of the steady state error between the grid power and boost power at 25°*C*.

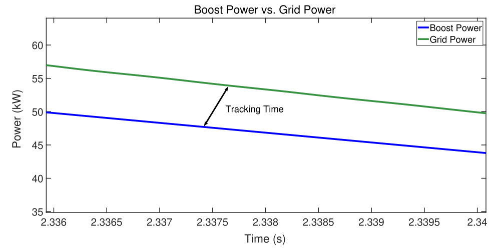

FIGURE 19. Simulation results of the tracking time between the grid power and boost power at 25°*C*.

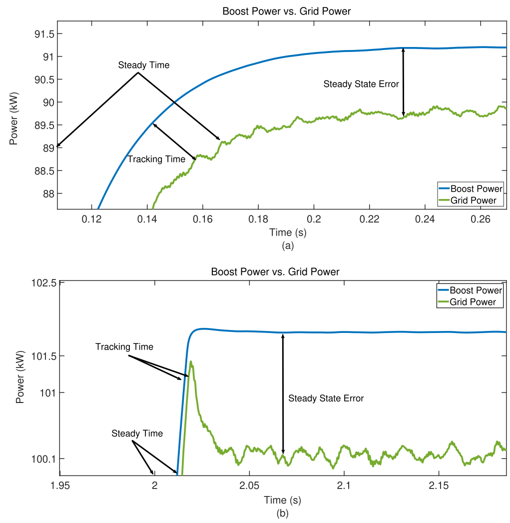

FIGURE 20. Errors between boost power and grid power at 40°C (a) and 20°C (b).

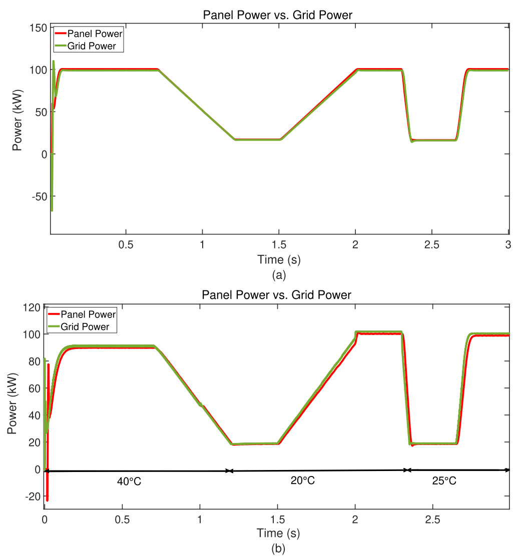

FIGURE 21. Simulation results of panel power and grid power at 25°*C* (a) and 40°*C*, 20°*C*, 25°*C* (b).

It is to be noted that even the steady state error for 40°C was less than 20°C the power transmitted from the panel to the grid was higher than those achieved in 40°C (i.e., 100.2kW and 89.8kW respectively). As regards *PV*-Boost simulations high accuracy and efficiency were reported (Fig. 13 - 15). The tracking time was 0.009s, the steady state error was 0.12 kW and the transit time was 0.08s for 25°C. For 20°C

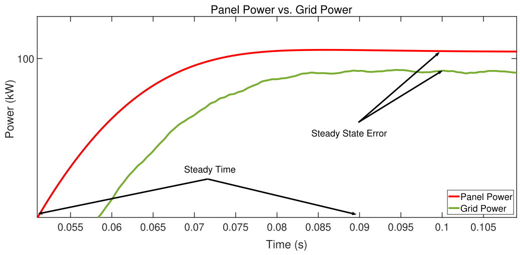

FIGURE 22. Simulation results of the steady time and steady state error of the grid power and PV Panel power at 25°C.

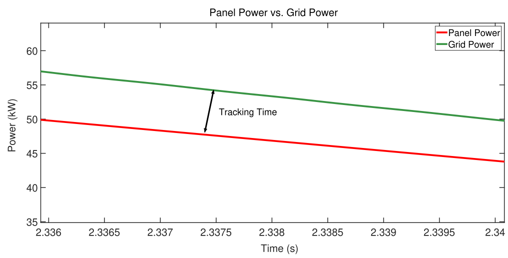

FIGURE 23. Simulation results of the tracking time between the grid power and PV panel power at 25°C.

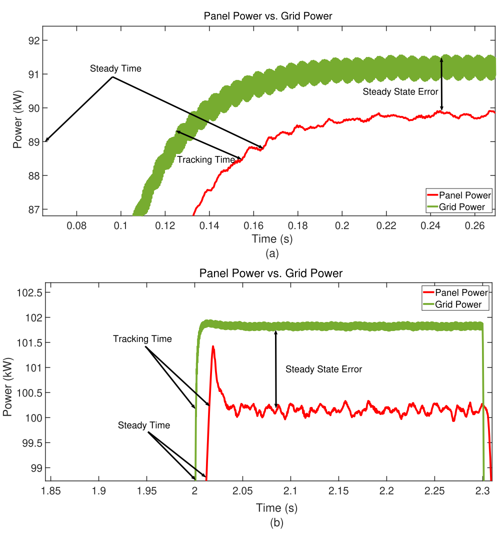

FIGURE 24. Errors between panel power and grid power at 40°C (a) and 20°C (b).

and 40°C the efficiencies are 99.99% and 90.7% respectively. This was due to: i) the use of few *MFs* which reduce the calculation time of the output; ii) the adequate, simple and fast choice of the duty cycle *D* by only two *MFs*. In relation to the results obtained between the boost and the grid at 25°C, a transit time of about 0.01s and a tracking time of 0.004s, were achieved (Fig.19). In Fig.18 the steady state error was of 1.71 kW which means an error of 1.69% for 20°C and 40°C. Fig. 20 (a) and (b) report, instead, the efficiency values that are 99.51% and 89.7% respectively. Most state-of-the-art works performed simulations at 25°C. For example, in [31], the best fuzzy system reported a transit time of 0.91s, a tracking accuracy of 99.93% with an error

TABLE 3. Summary of the comparative study.

Controllers	Efficiency %	Error %
TOANC	99.12	0.88
FLC	91.51	8.49
PID-IC	87.67	12.33
PID-HC	84.01	15.99

TABLE 4. Comparison of power efficiencies.

Controllers	Efficiency%	Error %
TOANC	99.12	0.88
Sliding mode controller	97.30	2.7
Integral Backstepping controller	98.04	1.96
Predictive	95.80	4.20
MPPT with irradiance sensor	98.62	1.38
P&O-ANFIS	85-97	15-3
Three-point weighted	96.00	4.00

TABLE 5. Summary of the comparative studies.

Controllers	Inputs	Steady State error	Tracking time	Architecture	Implementation
P&O	$\triangle P$ and $\triangle V$	until 10%	0.25s	Very Easy	Very Easy
ANN	GMPP and VGMPP	0.6%	0.05s	Difficult	Difficult
Neuro-Fuzzy	E and $\triangle E$	0.5%	0.5s	Heavy	Difficult
Fuzzy	$\triangle P$ and $\triangle V$	0.37%	0.91s	Quite Easy	Quite Easy
TOANC	W and $\triangle W$	0.88%	/	Heavy	Difficult
HRFLC	$\triangle I$	0.119%	0.008s	Very Easy	Very Easy

of 5.86Wh and a steady state error of 0.37%. The *P&O* (0.5%) in [31] reported a transit time of 0.25s and a steady state error of 7.16%. The *ANNs* used in the literature, the steady state error was approximately 3W for 30W (10% of error) [52]. The *ANN*-based system proposed in [53] provised a transit time of 0.05s with a steady stat error of 0.6%. In [54] the proposed fuzzy system reported a transit time of 0.25s, and a mean steady state error of 2.36%. In [22] using adaptive neuro-fuzzy controller the steady stat error was about 0.5%. In [24] the tracking time error estimated was 1.58s. For further evaluation, Table 3 illustrates the results presented in [45], [46] such as Third Order B-spline Adaptive Neuro-fuzzy Controller (*TOANC*), fuzzy logic controller, PID–incremental conductance (*PID–InCon*) and PID–Hill climbing (*PID–HC*). As can be observed, *TOANC* achieved the highest efficiency and the lowest error as it employed the *MPPT* error and its derivative.

Kamal *et al.* [45], [46] compared the proposed method *TOANC* with sliding mode controller, integral backstepping controller, predictive, *MPPT* with irradiance sensor, *ANFIS* and three point weighted. Comparative results are reported in Table 4. Hence, the proposed *HRFLC*-based *MPPT*, which achieved an efficiency of 99.12%, with only one input, one output, and two rules. This *FLC* can be easily implemented and widely used. Results are summarized Table 5.

TABLE 6. Results achieved for simulations carried out at 20°C and 40°C.

	40°C			20°C		
	PP/BP	BP/GP	PP/GP	PP/BP	BP/GP	PP/GP
IE	9.5kW	/	/	≈0	/	/
SSE	0.01kW	1.4kW	1.4kW	0.005kW	2kW	1.8kW
TT	0.01s	0.03s	0.04s	0.01s	0.005s	0.02s
ST	0.22s	0.17s	0.17s	0.04s	0.02s	0.02s

The results achieved for 20°C and 40°C are reported in Table 6.

The proposed *HRFLC* provided high performances with a reduced number of *MFs* and rules, making its architecture very simple. In fact, the main idea was to keep the voltage stable while the current control the irradiance variation. The choice of the single input $\triangle I$ simplifies considerably the implementation. The reasons of using $\triangle I$ can be summarized as follows: first, the voltage of the *VSC* must be kept constant and stable in order to supply the grid with fixed AC voltage. Second, the current is more sensible in the B-C zone than the other zones as this work deals with Boost controller. Third, components, time and memory are reduced significantly.

VIII. CONCLUSION

In this work, an *HRFLC*-based *MPPT* method is proposed as an accurate, simple and representative approach. The design and simulation of the method are discussed in detail. In this article, only the current variation is used under different weather conditions (i.e., irradiation at 20°C, 25°C and 40°C), achieving high accuracy and efficiency, by employing a number of inputs less than usually used in the literature, mainly twenty-five rules or over. This reduction means that the calculation is simplified significantly. Comparing to the conventional *P&O* method, the proposed *MPPT* method can satisfactorily address the trade-off between the tracking speed and steady state oscillations. Moreover, a connection to a grid is achieved. This connection provided high performances. Moreover, the use of Fuzzy in *MPPT* control (*HRFLC*) achieves better results than the classical approach, especially for static error and tracking time. Furthermore, in comparison with other controllers like fuzzy, *ANNs* and so on, the *HRFLC* reported higher accuracy and efficiency in tracking time, transit time, and steady state with a high reduction in variables and functions. This reduction allows not only to simplify the implementation process but also to achieve a significant gain in terms of time and cost (by using a smaller number of components). This will make an easy process for installation and maintenance. As an alternative perspective, in the future, exploitation of deep and/or reinforcement learning methods [13]–[18], [55] will be also explored.

REFERENCES

[1] J. Ahmed and Z. Salam, "A modified P&O maximum power point tracking method with reduced steady-state oscillation and improved tracking efficiency," *IEEE Trans. Sustain. Energy*, vol. 7, no. 4, pp. 1506–1515, Oct. 2016.

[2] H.-T. Yau and C.-H. Wu, "Comparison of extremum-seeking control techniques for maximum power point tracking in photovoltaic systems," *Energies*, vol. 4, no. 12, pp. 2180–2195, Dec. 2011.

[3] C. Li, Y. Chen, D. Zhou, J. Liu, and J. Zeng, "A high-performance adaptive incremental conductance MPPT algorithm for photovoltaic systems," *Energies*, vol. 9, no. 4, p. 288, Apr. 2016.

[4] Y. Sun, S. Li, B. Lin, X. Fu, M. Ramezani, and I. Jaithwa, "Artificial neural network for control and grid integration of residential solar photovoltaic systems," *IEEE Trans. Sustain. Energy*, vol. 8, no. 4, pp. 1484–1495, Oct. 2017.

[5] M. A. Elgendy, B. Zahawi, and D. J. Atkinson, "Assessment of perturb and observe MPPT algorithm implementation techniques for PV pumping applications," *IEEE Trans. Sustain. Energy*, vol. 3, no. 1, pp. 21–33, Jan. 2012.

[6] S. Strache, J. H. Mueller, D. Platz, R. Wunderlich, and S. Heinen, "Maximum power point tracker for small number of solar cells connected in series," in *Proc. 38th Annu. Conf. IEEE Ind. Electron. Soc. IECON*, Oct. 2012, p. 5732.

[7] J. T. Bialasiewicz, "Renewable energy systems with photovoltaic power generators: Operation and modeling," *IEEE Trans. Ind. Electron.*, vol. 55, no. 7, pp. 2752–2758, Jul. 2008.

[8] Y. Jiang, J. A. Abu Qahouq, and T. A. Haskew, "Adaptive step size with adaptive-perturbation-frequency digital MPPT controller for a single-sensor photovoltaic solar system," *IEEE Trans. Power Electron.*, vol. 28, no. 7, pp. 3195–3205, Jul. 2013.

[9] S. K. Kollimalla and M. K. Mishra, "Variable perturbation size adaptive P&O MPPT algorithm for sudden changes in irradiance," *IEEE Trans. Sustain. Energy*, vol. 5, no. 3, pp. 718–728, Jul. 2014.

[10] Q. Mei, M. Shan, L. Liu, and J. M. Guerrero, "A novel improved variable step-size incremental-resistance MPPT method for PV systems," *IEEE Trans. Ind. Electron.*, vol. 58, no. 6, pp. 2427–2434, Jun. 2011.

[11] A. I. Dounis, P. Kofinas, C. Alafodimos, and D. Tseles, "Adaptive fuzzy gain scheduling PID controller for maximum power point tracking of photovoltaic system," *Renew. Energy*, vol. 60, pp. 202–214, Dec. 2013.

[12] M. Mazandarani and X. Li, "Fractional fuzzy inference system: The new generation of fuzzy inference systems," *IEEE Access*, vol. 8, pp. 126066–126082, 2020.

[13] M. Mahmud, M. S. Kaiser, A. Hussain, and S. Vassanelli, "Applications of deep learning and reinforcement learning to biological data," *IEEE Trans. Neural Netw. Learn. Syst.*, vol. 29, no. 6, pp. 2063–2079, Jan. 2018.

[14] C. Ieracitano, N. Mammone, A. Hussain, and F. C. Morabito, "A novel multi-modal machine learning based approach for automatic classification of EEG recordings in dementia," *Neural Netw.*, vol. 123, pp. 176–190, Mar. 2020.

[15] N. Mammone, C. Ieracitano, and F. C. Morabito, "A deep CNN approach to decode motor preparation of upper limbs from time–frequency maps of EEG signals at source level," *Neural Netw.*, vol. 124, pp. 357–372, Apr. 2020.

[16] Z. K. Malik, A. Hussain, and Q. J. Wu, "Multilayered echo state machine: A novel architecture and algorithm," *IEEE Trans. Cybern.*, vol. 47, no. 4, pp. 946–959, Apr. 2017.

[17] F. Xiong, B. Sun, X. Yang, H. Qiao, K. Huang, A. Hussain, and Z. Liu, "Guided policy search for sequential multitask learning," *IEEE Trans. Syst., Man, Cybern. Syst.*, vol. 49, no. 1, pp. 216–226, Jan. 2019.

[18] X. Yang, K. Huang, R. Zhang, and A. Hussain, "Learning latent features with infinite nonnegative binary matrix trifactorization," *IEEE Trans. Emerg. Topics Comput. Intell.*, vol. 2, no. 6, pp. 450–463, Dec. 2018.

[19] M. S. Kaiser, Z. I. Chowdhury, S. A. Mamun, A. Hussain, and M. Mahmud, "A neuro-fuzzy control system based on feature extraction of surface electromyogram signal for solar-powered wheelchair," *Cognit. Comput.*, vol. 8, no. 5, pp. 946–954, Oct. 2016.

[20] M. Mahmud, M. S. Kaiser, M. M. Rahman, M. A. Rahman, A. Shabut, S. Al-Mamun, and A. Hussain, "A brain-inspired trust management model to assure security in a cloud based IoT framework for neuroscience applications," *Cognit. Comput.*, vol. 10, no. 5, pp. 864–873, Oct. 2018.

[21] H. Seiti and A. Hafezalkotob, "A new risk-based fuzzy cognitive model and its application to decision-making," *Cognit. Comput.*, vol. 12, no. 1, pp. 309–326, Jan. 2020.

[22] M. Mahdavi, L. Li, J. Zhu, and S. Mekhilef, "An adaptive neuro-fuzzy controller for maximum power point tracking of photovoltaic systems," in *Proc. TENCON IEEE Region Conf.*, Nov. 2015, pp. 1–6. [Online]. Available: https://umexpert.um.edu.my/file/publication/00005361_133573.pdf

[23] S. S. Mohammed, D. Devaraj, and T. P. I. Ahamed, "Maximum power point tracking system for stand alone solar PV power system using adaptive neuro-fuzzy inference system," in *Proc. Biennial Int. Conf. Power Energy Syst., Towards Sustain. Energy (PESTSE)*, Jan. 2016, pp. 1–4.

[24] A. Bin-Halabi, A. Abdennour, and H. Mashaly, "An accurate ANFIS-based MPPT for solar PV system," *Int. J. Adv. Comput. Res.*, vol. 4, no. 2, p. 588, 2014.

[25] S. Tang, Y. Sun, Y. Chen, Y. Zhao, Y. Yang, and W. Szeto, "An enhanced MPPT method combining fractional-order and fuzzy logic control," *IEEE J. Photovolt.*, vol. 7, no. 2, pp. 640–650, Mar. 2017.

[26] L. K. Letting, J. L. Munda, and Y. Hamam, "Optimization of a fuzzy logic controller for PV grid inverter control using S-function based PSO," *Sol. Energy*, vol. 86, no. 6, pp. 1689–1700, Jun. 2012.

[27] M. M. Algazar, H. Al-Monier, H. A. El-halim, and M. E. El Kotb Salem, "Maximum power point tracking using fuzzy logic control," *Int. J. Elect. Power Energy Syst.*, vol. 39, no. 1, pp. 21–28, 2012.

[28] B. N. Alajmi, K. H. Ahmed, S. J. Finney, and B. W. Williams, "Fuzzy-logic-control approach of a modified hill-climbing method for maximum power point in microgrid standalone photovoltaic system," *IEEE Trans. Power Electron.*, vol. 26, no. 4, pp. 1022–1030, Apr. 2011.

[29] B. N. Alajmi, K. H. Ahmed, S. J. Finney, and B. W. Williams, "A maximum power point tracking technique for partially shaded photovoltaic systems in microgrids," *IEEE Trans. Ind. Electron.*, vol. 60, no. 4, pp. 573–584, Apr. 2013.

[30] C. B. Alah and M. Ouali, "Comparison of fuzzy logic and neural network in maximum power point tracker for PV systems," *Electr. Power Syst. Res.*, vol. 81, no. 1, pp. 43–50, Jan. 2011.

[31] C.-L. Liu, J.-H. Chen, Y.-H. Liu, and Z.-Z. Yang, "An asymmetrical fuzzy-logic-control-based MPPT algorithm for photovoltaic systems," *Energies*, vol. 7, no. 4, pp. 2177–2193, Apr. 2014.

[32] J.-K. Shiau, Y.-C. Wei, and B.-C. Chen, "A study on the fuzzy-logic-based solar power MPPT algorithms using different fuzzy input variables," *Algorithms*, vol. 8, no. 2, pp. 100–127, Apr. 2015.

[33] T. K. Mohan and S. F. Mohammed, "A neuro-fuzzy controller for multilevel renewable energy system," in *Proc. Int. Conf. Electr., Electron., Optim. Techn. (ICEEOT)*, Mar. 2016, pp. 4120–4123.

[34] M. Barsacchi, A. Bechini, P. Ducange, and F. Marcelloni, "Optimizing partition granularity, membership function parameters, and rule bases of fuzzy classifiers for big data by a multi-objective evolutionary approach," *Cognit. Comput.*, vol. 11, no. 3, pp. 367–387, Jun. 2019.

[35] S. López, A. A. Márquez, F. A. Márquez, and A. Peregrín, "Evolutionary design of linguistic fuzzy regression systems with adaptive defuzzification in big data environments," *Cognit. Comput.*, vol. 11, no. 3, pp. 388–399, Jun. 2019.

[36] L. Zhang and Y. He, "Extensions of intuitionistic fuzzy geometric interaction operators and their application to cognitive microcredit origination," *Cognit. Comput.*, vol. 11, no. 5, pp. 748–760, Oct. 2019.

[37] X. Tang and G. Wei, "Multiple attribute decision-making with dual hesitant pythagorean fuzzy information," *Cognit. Comput.*, vol. 11, no. 2, pp. 193–211, Apr. 2019.

[38] G. Sun, X. Guan, X. Yi, and Z. Zhou, "Improvements on correlation coefficients of hesitant fuzzy sets and their applications," *Cognit. Comput.*, vol. 11, no. 4, pp. 529–544, Aug. 2019.

[39] L. M. Elobaid, A. K. Abdelsalam, and E. E. Zakzouk, "Artificial neural network based maximum power point tracking technique for PV systems," in *Proc. 38th Annu. Conf. IEEE Ind. Electron. Soc. IECON*, Oct. 2012, pp. 937–942.

[40] A. M. Ameen, J. Pasupuleti, T. Khatib, W. Elmenreich, and H. A. Kazem, "Modeling and characterization of a photovoltaic array based on actual performance using cascade-forward back propagation artificial neural network," *J. Sol. Energy Eng.*, vol. 137, no. 4, Aug. 2015.

[41] E. Karatepe and T. Hiyama, "Artificial neural network-polar coordinated fuzzy controller based maximum power point tracking control under partially shaded conditions," *IET Renew. Power Generat.*, vol. 3, no. 2, pp. 239–253, 2009.

[42] V. Salas, E. Olías, A. Lázaro, and A. Barrado, "New algorithm using only one variable measurement applied to a maximum power point tracker," *Sol. Energy Mater. Sol. Cells*, vol. 87, nos. 1–4, pp. 675–684, May 2005.

[43] S. B. Jeyaprabha and A. I. Selvakumar, "Model-based MPPT for shaded and mismatched modules of photovoltaic farm," *IEEE Trans. Sustain. Energy*, vol. 8, no. 4, pp. 1763–1771, Oct. 2017.

[44] N. S. D'Souza, L. A. C. Lopes, and X. Liu, "Comparative study of variable size perturbation and observation maximum power point trackers for PV systems," *Electr. Power Syst. Res.*, vol. 80, no. 3, pp. 296–305, Mar. 2010.

[45] T. Kamal, M. Karabacak, F. Blaabjerg, S. Z. Hassan, and L. M. Fernández-Ramírez, "A novel Lyapunov stable higher order B-spline online adaptive control paradigm of photovoltaic systems," *Sol. Energy*, vol. 194, pp. 530–540, Dec. 2019.

[46] T. Kamal, M. Karabacak, S. Z. Hassan, H. Li, and L. M. Fernandez-Ramirez, "A robust online adaptive B-Spline MPPT control of three-phase grid-coupled photovoltaic systems under real partial shading condition," *IEEE Trans. Energy Convers.*, vol. 34, no. 1, pp. 202–210, Mar. 2019.

[47] A. Haque, "Maximum power point tracking (MPPT) scheme for solar photovoltaic system," *Energy Technol. Policy*, vol. 1, no. 1, pp. 115–122, Jan. 2014.

[48] M. Merenda, D. Iero, R. Carotenuto, and F. G. D. Corte, "Simple and low-cost photovoltaic module emulator," *Electronics*, vol. 8, no. 12, p. 1445, Dec. 2019.

[49] S. K. Chattopadhyay and C. Chakraborty, "A new asymmetric multilevel inverter topology suitable for solar PV applications with varying irradiance," *IEEE Trans. Sustain. Energy*, vol. 8, no. 4, pp. 1496–1506, Oct. 2017.

[50] K. R. M. N. Ratnayake, Y. Murai, and T. Watanabe, "Novel PWM scheme to control neutral point voltage variation in three-level voltage source inverter," in *Proc. Conf. Rec. IEEE Ind. Appl. Conf., 34th IAS Annu. Meeting*, vol. 3, Oct. 1999, pp. 1950–1955.

[51] A.-C. Rufer, "An aid in the teaching of multilevel inverters for high power applications," in *Proc. PESC Power Electron. Specialist Conf.*, Jun. 1995, pp. 347–352.

[52] H. Zhang and S. Cheng, "A new MPPT algorithm based on ANN in solar PV systems," in *Advances in Computer, Communication, Control and Automation* (Lecture Notes in Electrical Engineering), vol. 121, Y. Wu, Ed. Berlin, Germany: Springer, 2011, pp. 77–84.

[53] L. Bouselham, M. Hajji, B. Hajji, and H. Bouali, "A MPPT-based ANN controller applied to PV pumping system," in *Proc. Int. Renew. Sustain. Energy Conf. (IRSEC)*, Nov. 2016, pp. 86–92.

[54] A. A. S. Mohamed, A. Berzoy, and O. A. Mohammed, "Design and hardware implementation of FL-MPPT control of PV systems based on GA and small-signal analysis," *IEEE Trans. Sustain. Energy*, vol. 8, no. 1, pp. 279–290, Jan. 2017.

[55] C. Ieracitano, N. Mammone, A. Bramanti, A. Hussain, and F. C. Morabito, "A convolutional neural network approach for classification of dementia stages based on 2D-spectral representation of EEG recordings," *Neurocomputing*, vol. 323, pp. 96–107, Jan. 2019.

LOTFI FARAH received the B.Eng. and Ph.D. degrees in Arabic handwritten recognition from Badji Mokhtar University, Annaba, Algeria, in 1995 and 2000, respectively. From 2000 to 2012, he was a Research Associate with the University of Souk Ahras Mohamed Chérif Messaadia, Algeria. He is currently a Researcher with the Génie Electromécanique Laboratory, Badji Mokhtar University. He has authored or coauthored different seminar articles. His current research interests include AI, fuzzy systems, neural network and photovoltaic modeling and control, and energy conversion and power electronics. He has reviewed for international journals in his research field, AI, such as *Environmental Progress and Sustainable Energy* journal (Wiley) and *Computer Science*, USA.

AMIR HUSSAIN (Senior Member, IEEE) received the B.Eng. (Hons.) and Ph.D. degrees from the University of Strathclyde, Glasgow, U.K., in 1992 and 1997, respectively. Following post-doctoral and academic positions at the University of West of Scotland from 1996 to 1998, University of Dundee from 1998 to 2000, and University of Stirling from 2000 to 2018, he joined Edinburgh Napier University, Scotland, U.K., in 2018, as the Founding Director of the Centre of AI and Data Science. He has (co)authored three international patents and over 400 publications, including 170+ international journal articles, 20 books/monographs, and over 100 book chapters. He has led major national, EU, and internationally funded projects, and supervised over 30 Ph.D. students and 30+ postdoctoral researchers to-date. His research interests include cross-disciplinary and industry-led, aimed at developing cognitive data science and AI technologies, to engineer the smart and secure systems of tomorrow. He has been the General Chair of the IEEE WCCI 2020 (the world's largest technical event in computational intelligence, comprising IJCNN, IEEE CEC, and FUZZ-IEEE), the Vice-Chair of the Emergent Technologies Technical Committee of the IEEE Computational Intelligence Society (CIS), the IEEE U.K. and Ireland Chapter Chair of the Industry Applications Society, and the (founding) Vice-Chair of the IEEE CIS Task Force on Intelligence Systems for e-Health. He is the Founding Editor-in-Chief of two leading international journals: *Cognitive Computation* (Springer Nature) and *Big Data Analytics* (BioMed Central), and the Springer Book Series on Socio-Affective Computing and Cognitive Computation Trends. He has been an Invited Associate Editor/Editorial Board Member for a number of other top journals, including the IEEE Transactions on Neural Networks and Learning Systems, *Information Fusion* (Elsevier), the IEEE Transactions on Systems, Man and Cybernetics: Systems, and the IEEE Transactions on Emerging Topics in Computational Intelligence.

ABDELFATEH KERROUCHE (Member, IEEE) received the M.Phil. degree in electronics from Pierre and Marie Curie Paris VI University, France, the master's degree in electronics from the University of Paris-Est Marne-la-Vallée, France, and the Ph.D. degree in measurement and instrumentation from the City, University of London, in 2009, funded by the Sustainable Bridges EU Project. From 2010 to 2015, he worked as a Research Associate with Heriot-Watt University. He developed 3-D ray-tracing models for luminescent solar concentrators and he designed systems for water sampling and pathogen detection within the Aqua Valens EU Project. Since 2016, he has been a Lecturer and a Sensors/Systems Consultant with Edinburgh Napier University. He has published more than 15 papers in reputed journals and international conferences. His research interests include pathogen detection, water sample preparation, sensors, aquaculture, and renewable energy.

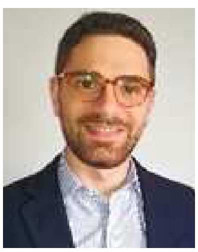

COSIMO IERACITANO received the master's degree *(summa cum laude)* in electronic engineering and the Ph.D. degree (with the additional label of Doctor Europaeus) from the Mediterranea University of Reggio Calabria, Italy, in 2013 and 2019, respectively. He was a Visiting Master Student with ETH Zürich and a Visiting Ph.D. Student with the University of Stirling, in 2013 and 2018, respectively. He is the author/coauthor of publications in peer-reviewed national/international journals and conference contributions. His main research interests include information theory, machine learning, deep learning techniques, and biomedical signal processing, in particular EEG signals of subjects affected by neuropathologies.

JAMIL AHMAD (Senior Member, IEEE) received the M.Sc. degree in information technology from the University of Warwick, U.K., the M.Sc. degree in computer science from the University of Peshawar, and the Ph.D. degree in artificial neural network from the Department of Electrical and Electronics Engineering, King's College London, U.K. He is currently holding the position of the Vice Chancellor at the Kohat University of Science and Technology (KUST), Kohat, Pakistan. He has over 22 years of Post-Ph.D. experience of administration, research, teaching, and project management at various international academic institutions. He has published over 110 papers/book chapters in the areas of science, engineering, and technology in international journals and refereed conferences. He is a Fellow of the British Computer Society, a Chartered Engineer (CEng), and a member of IET and ACM. He received grants for his research and academic projects from various organizations, including the National Information and Communication Technology (ICT) Research and Development Fund, Pakistan, the HEC-British Council Linkage Program, and the U.K. Government under PMI 2 Program. He was a recipient of the Charles Wallace Pakistan Trust Visiting Fellowship, U.K., from 2012 to 2013, and the International Visiting Leadership Program (IVLP) Fellowship, from August 2007 to September 2007, USA.

MUFTI MAHMUD (Senior Member, IEEE) received the Ph.D. degree in information engineering from the University of Padua, Padua, Italy, in 2011. He is currently a Senior Lecturer with the Department of Computing and Technology, School of Science and Technology, Nottingham Trent University, U.K. With over 70 peer-reviewed research articles, his current research interests include neuroscience big data analytics, the Internet of healthcare things, and trust management in cyber-physical systems. He serves as an Editorial Board Member of *Cognitive Computation* (Springer-Nature) and *Big Data Analytics* (BioMed Central, Springer-Nature) journals. He was a recipient of the Marie-Curie Fellowship. He also serves at various capacities in the organization of leading conferences, including the Coordinating Chair of the Local Organization Committee of the IEEE WCCI2020 Conference and the General Chair of the Brain Informatics 2020 Conference. He serves as an Associate Editor for *Brain Informatics* (SpringerOpen) and IEEE Access journals.